Multilayer and Surface Immobilization of EDOT-Decorated Nanocapsules

Hambly, Bradley; Sears, Chandler; Guzinski, Marcin; Perez, Felio; Latonen, Rose-Marie; Bobacka, Johan; Pendley, Bradford; Lindner, Ernö

Published in:
Langmuir

DOI:
10.1021/acs.langmuir.0c03160

Published: 29/12/2020

Document Version
Accepted author manuscript

Multilayer and Surface Immobilization of EDOT-decorated Nanocapsules

Bradley P. Hambly[1], Chandler K. Sears[1], Marcin Guzinski[2], Felio Perez[3], Rose-Marie Latonen[4], Johan Bobacka[4], Bradford D. Pendley,[1] Ernő Lindner[1,*]

1: Department of Biomedical Engineering, University of Memphis, Memphis, TN 38152, USA

2: Vanderbilt Eye Institute, Vanderbilt University Medical Center, Nashville TN, 37232

3: Material Science Lab, Integrated Microscopy Center, University of Memphis, Memphis, TN 38152, USA

4: Johan Gadolin Process Chemistry Centre, Laboratory of Molecular Science and Engineering, Åbo Akademi University, FI-20500 Turku/Åbo, Finland

[*] Corresponding author: elindner@memphis.edu

Abstract

To assess the feasibility of utilizing reagent-loaded, porous polymeric nanocapsules (NCs) for chemical and biochemical sensor design, the surfaces of the NCs were decorated with 3,4-ethylenedioxythiophene (EDOT) moieties. The pores in the capsule wall allow unhindered bidirectional diffusion of molecules smaller than the programmed pore sizes, while larger molecules are either entrapped inside or blocked from entering the interior of the nanocapsules. Here we investigate two electrochemical deposition methods to covalently attach acrylate-based porous nanocapsules with 3,4-ethylenedioxythiophene (EDOT) moieties on the nanocapsule surface, i.e. EDOT-decorated NCs to the surface of an existing PEDOT film: (1) galvanostatic or bilayer deposition with supporting EDOT in the deposition solution and (2) potentiostatic deposition without supporting EDOT in the deposition solution. The distribution of the covalently attached NCs in the PEDOT films was studied by variable angle FTIR-ATR and XPS depth profiling. The galvanostatic deposition of EDOT-decorated NCs over an existing PEDOT(tetrakis(pentafluorophenyl)borate) [PEDOT(TPFPhB)] film resulted in a bilayer structure, with an interface between the NC-free and NC-loaded layers, that could be traced with variable angle FTIR-ATR measurements. In contrast, the FTIR-ATR and XPS analysis of the films deposited potentiostatically from a solution without EDOT and containing only the EDOT-decorated NCs showed small amounts of NCs in the entire cross-section of the films.

Introduction

Cationic and anionic surfactants in particular ratios and in the presence of acrylate monomers, preferentially self-assemble into vesicles with the monomer populating the hydrophobic region of the vesicles.[1] The hydrophobic region of the surfactant vesicles can be further loaded with free-radical UV initiators and hydrophobic non-reactive pore-forming templates, e.g., glucose pentaacetate (GPA) or glucose pentabenzoate (GPB)[2] (Figure 1a).The flexible vesicles can be resized by extrusion through a track-etched membrane (Figure 1b). Upon UV polymerization, the monomers located in the vesicle bilayer form a polymeric shell or nanocapsule (NC) with a single nanometer-thin wall[3] (Figure 1c). When the pore-forming templates are removed, hollow NCs with porous walls remain behind (Figure 1d). The pore sizes and pore density in the NC wall can be tuned through the appropriate selection of the pore-forming template and its concentration. The interior of the NCs can be loaded with a range of compounds either by encapsulation before the polymerization of the porous walls, as shown in Figure 1, or following the polymerization of the porous walls by in situ synthesis in the interior of the NCs.[4-5] The loaded NCs with porous walls have been used as drug delivery devices, ratiometric thermometers, catalyst-loaded nanoreactors, and as optical sensing particles.[6-9] Due to the nanometer-thin walls of the NCs, diffusion of ions and small molecules through the capsule wall is practically unhindered. The unhindered diffusion was confirmed by response time measurements in a stopped-flow manifold using free and encapsulated fluorescent dyes.[10]

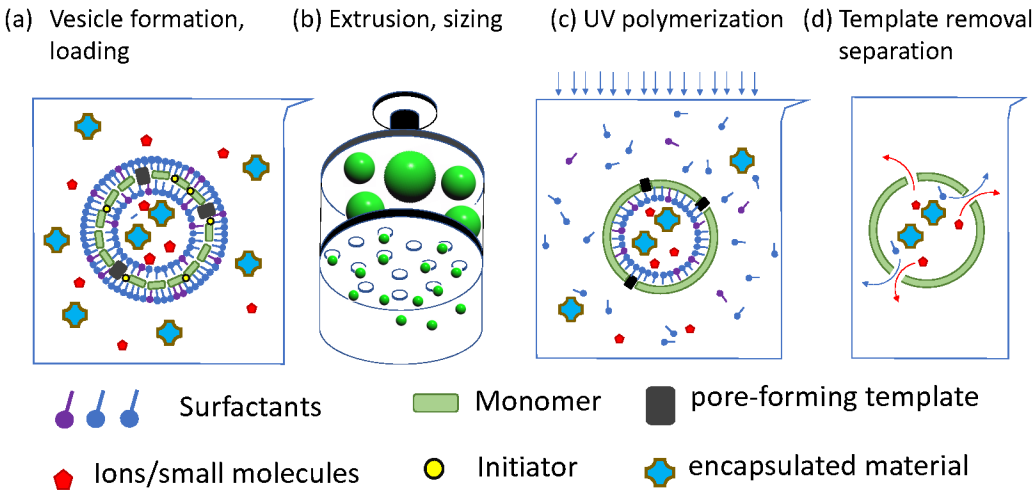

Figure 1: Schematic representation of the synthesis of reagent-loaded porous NCs using self-assembled surfactant vesicles as templates. (a) Vesicle formation in the presence of acrylate monomer, free-radical UV initiator, pore forming template, and molecules for encapsulation, (b) Repeated extrusion across a 100 nm pore size track-etched membrane, (c) UV light activated photo-polymerization of the acrylate monomer in the hydrophobic region of the surfactant bilayer, (d) Removal of the pore forming templates from the walls of the NCs and separation of the reagent-loaded NCs.

However, when pH-sensitive dye-loaded NCs were embedded (immobilized) in a polyvinyl alcohol hydrogel matrix, the extremely short response time experienced with the free-floating NCs was lost, and diffusion in the supporting matrix dominated the rate of response.[8] Recently, we became interested in the feasibility of direct attachment of the hollow NCs with porous walls to a sensing surface. While several methods have been used for surface immobilization of nanoparticles, e.g., click- and thiol-gold chemistry,[11-12] immobilization onto conductive polymers offers unique advantages, especially for designing electrochemical sensors. The possibility of site-specific electrochemical deposition of conductive polymers (CPs) is a significant advantage in building multianalyte, miniature sensor arrays.[13] Nanomaterial-doped

conducting polymers are important in electrochemical and biosensors development.[14] Since the introduction of poly(3,4-ethylenedioxythiophene) as an ion-to-electron transducer in solid contact ion-selective electrodes,[15] conductive polymers have been used in the design of novel potentiometric sensors.[16-18] To combine the benefits of the reagent-loaded hollow NCs with the convenience and broad-ranging application possibilities of conducting polymers, we have synthesized hollow NCs from an acrylate linked 3,4-ethylenedioxythiophene (EDOT-AA) monomer, i.e., the surfaces of these NCs are decorated with EDOT moieties.[19] The incorporation of EDOT moieties in the walls of the NCs when EDOT-AA is used for the NC synthesis was confirmed by FTIR-ATR spectroscopy.[19] The EDOT moieties on the NC surfaces could be co-polymerized with free EDOT molecules during the electrochemical deposition of PEDOT films. Figure 2a is a schematic representation how the EDOT-decorated NCs are coupled to an electrochemically deposited PEDOT-film. The SEM image in Figure 2b shows the surface of a PEDOT film which has been electrochemically deposited in the presence of EDOT-decorated polymeric capsules with diameters ranging between ~ 0.4 and ~2.0 µm. The sizes of the polymeric capsules are so large because the capsule walls were polymerized (Figure 1c) without sizing the capsules by repeated extrusion (Figure 1b). Such large capsules were used to record the image of Figure 2b intentionally, because in the spongy structure of the electrochemically deposited PEDOT film NCs with 100 to 200 nm diameter are hardly recognizable. An SEM image of a PEDOT(tetrakis(pentafluorophenyl)borate) [PEDOT(TPFPhB)] film which has been electrochemically deposited in the presence of ~ 100 nm diameter EDOT-decorated polymeric capsules is shown in Figure S1 of the supporting information.

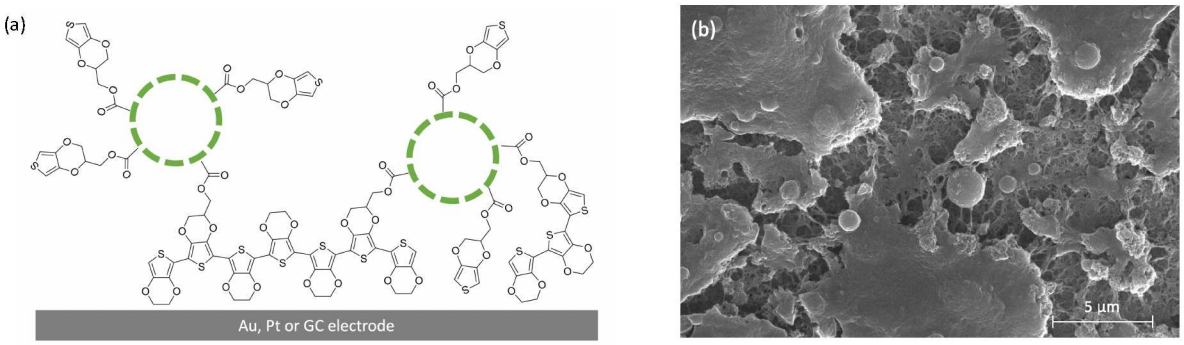

Figure 2: (a) Schematic representation of the covalent attachment of EDOT-decorated NCs to an electrochemically deposited PEDOT film. (b) SEM image of a PEDOT(TPFPhB) film which was deposited in the presence of EDOT-decorated polymeric capsules with diameters ranging between ~ 0.4 and ~2.0 µm.

Experimental

Reagents

The chemicals used in the synthesis of the EDOT-decorated NCs were hexadecyltrimethylammonium p-toluenesulfonate (CTAT), sodium dodecylbenzenesulfonate (SDBS), ethylene glycol dimethacrylate (EGDMA), tert-butyl methacrylate (t-BMA), butyl methacrylate (BMA), glucose pentaacetate (GPA), 2,2-dimethoxy-2-phenyl-acetophenone (DPA), and 2'-methyl acrylate-3,4-ethylenedioxythiophene (EDOT-AA), and all were purchased from Sigma-Aldrich with the exception of EDOT-AA which was synthesized in our lab.[19] Before use, the inhibitor in the acrylate monomers (t-BMA, BMA, and EGDMA) were removed by filtration through a 2-inch alumina column (Fluka 06300, aluminum oxide for chromatography). The chemicals used in the synthesis of EDOT-AA were 3,4-dimethoxythiophene (DMT), 3-chloro-1,2-propanediol (ChPD), acrylic acid (AA), K_2CO_3, and KI which were purchased from Sigma-Aldrich. For the deposition of the conductive polymers, 3,4-ethylenedioxythiophene (EDOT)

monomer was polymerized using tetrakis(pentafluorophenyl)borate ($TPFPhB^-$), poly(4-styrenesulfonate) (PSS) and chloride (Cl^-) as the doping anions in the form of KTPFPhB, Na(PSS) and KCl. Both EDOT and KTPFPhB were purchased from Sigma-Aldrich, Na(PSS) was purchased from Acros Organics and KCl was purchased from Fisher. Ferrocene methanol (FcMeOH), from Sigma Aldrich, was used for the electrochemical characterization of the PEDOT film coated electrodes. All the solvents used in the synthesis, separation and purification steps of the synthesis and the deposition of the EDOT films (toluene, hexane, dichloromethane (DCM), dimethyl sulfoxide (DMSO), ethyl acetate, methanol, chloroform, acetonitrile) were from Sigma Aldrich. Aqueous solutions were prepared with 18.2 MΩcm resistivity deionized water from a Millipore Milli-Q A10 system.

Synthesis

For the synthesis of 2'-chloromethyl-3,4-ethylenedioxy-thiophene (EDOT-Cl) and 2'-methyl acrylate-3,4-ethylenedioxy-thiophene (EDOT-AA), we followed previously published protocol with slight modifications.[20-21] The modifications in the protocol are provided on page 6329 in our previous paper.[19] Similarly, the synthesis of the EDOT-decorated hollow NCs and the in-situ synthesis of iron (II) tris(bipyridine) complex ($Fe(bpy)_3$) inside of the porous NCs (page 6330) have been described in our previous paper.[19] The structures of the synthesized materials have been confirmed by ^{1}H-NMR and FTIR-ATR. The presence of $Fe(bpy)_3$ complex inside of the hollow NCS was confirmed by XPS. The size distribution of the NCs was determined by dynamic light scattering (DLS) measurements.

Instruments and Methods

Electrode Preparation: The PEDOT films were deposited on ITO coated glass slides (≤10 Ω/square, Präzisions Glas & Optik) or either gold (Au) or glassy carbon (GC) electrodes (3 mm diameter, MF-1002 or MF-2012, Bioanalytical System, Inc., West Lafayette, IN). The ITO coated glass slides were used for the FTIR-ATR studies, the Au electrodes were used for XPS analysis and the GC electrodes were used for the electrochemical characterization of the PEDOT films. The Au and GC electrodes were polished on microcloth polishing pads (Buehler, Lake Bluff, IL) before use using Buehler Al_2O_3 slurries with 1.0, 0.3 and 0.05 µm grain sizes. Between polishing steps, the electrodes were washed with DI water. After the final polishing step with the 0.05 µm slurry, the electrodes were sonicated twice for 10 min in soapy water and three times 10 min in DI water, with DI water rinsing between each sonication. ITO coated glass slides were used as received but were cleaned by sonicating the electrodes in methanol for 10 min, followed by sonication in DI water for 10 min and a final acetonitrile rinse before use.

Deposition of EDOT-Decorated Nanocapsules into the Bulk and to the Surface of PEDOT Films: PEDOT films were co-polymerized with the EDOT-decorated NCs with three different methods, shown in Figure 3. The aim of this paper is to explore the possibility of depositing the EDOT-decorated NCs to the surface layers of existing PEDOT films.

Bulk Deposition (Figure 3a): PEDOT(TPFPhB) films were deposited galvanostatically at 0.2 mA/cm^2 current density onto ITO coated glass slides or Au or GC electrode surfaces in a three-electrode electrochemical cell using PGSTAT 20 (Metrohm Autolab Inc.). The PEDOT(PSS) and PEDOT(Cl) films were deposited under the same conditions onto GC electrode surfaces. The

deposition times varied depending on the required film thickness. 714 s electrolysis time resulted in approximately 1 μm thick PEDOT(TPFPhB) films.[22] In the electrochemical cell, platinum wire and glassy carbon rod served as the quasi-reference (0.275 V vs. sat. Ag/AgCl in 0.1 M KCl) and counter electrodes, respectively. The polymerization solution contained 10 mg/mL EDOT-decorated NCs, 0.03 M KTPFPhB and 0.015 M EDOT in 20 % acetonitrile – 80% water mixture. An example of the potential vs. time recording during the galvanostatic deposition is shown in Figure S2 of the supporting information. Following the deposition, the films were rinsed with 5 × 5 mL acetonitrile and left for one hour to dry.

Surface deposition; Galvanostatic/Bilayer Deposition (Figure 3b): For the galvanostatic/bilayer deposition of the EDOT-decorated NCs first, an approximately 1 μm thick PEDOT(TPFPhB) film was deposited galvanostatically on an ITO glass slide or an Au electrode in the same electrochemical cell, galvanostatic current density and electrolysis time (0.2 mA/cm^2 for 714s) as it was described above. Following the PEDOT(TPFPhB) film deposition, a ~ 0.5 μm thick copolymer film was deposited with the same current density and 356 s electrolysis time in a solution containing 10 mg/mL EDOT-decorated NCs as well as 0.03 M KTPFPhB, and 0.015 M EDOT in an acetonitrile/water mixture (20 % acetonitrile). During the electrochemical deposition of the NCs onto the top ~ 0.5 μm thick PEDOT(TPFPhB) film, the orientation of the electrode surfaces ensured that the incorporation of NCs is not biased by NC sedimentation. Following each deposition step, the electrodes were rinsed with at least 3 × 20 mL of acetonitrile.

Surface deposition; Potentiostatic Deposition (Figure 3c): For the potentiostatic deposition of the EDOT-decorated NCs, first an approximately 1 μm thick PEDOT(TPFPhB) film was

deposited galvanostatically (0.2 mA/cm^2 for 714 s) on an ITO coated glass slide or Au electrode in the same manner as described above. Next, the PEDOT(TPFPhB) film was carefully rinsed with 5×5 mL of acetonitrile, and the deposition of the EDOT-decorated NCs to the PEDOT(TPFPhB) film was attempted potentiostatically from a solution containing only 10 mg/mL EDOT-decorated NCs and 0.03 M KTPFPhB, but no EDOT. For the potentiostatic deposition, a potential of 1.2 V was applied for 1200s vs a platinum quasi-reference electrode. The potential of the Pt quasi-reference electrode in 0.1 M KCl was 0.275 V vs. sat. Ag/AgCl, i.e., during the potentiostatic deposition the working electrode potential was ~ 0.925 V vs. a sat. Ag/AgCl electrode. The electrodes were then rinsed again 3×20 mL of acetonitrile and left to dry for one hour. An example of the current vs. time recording during the potentiostatic deposition is shown in Figure S3 of the supporting information.

Cyclic voltammetry and Impedance spectroscopy: To show the unique electrochemical characteristics of the PEDOT(TPFPhB) coated GC electrodes in comparison to GC electrodes coated by PEDOT(PSS) and PEDOT(Cl) cyclic voltammetry and impedance spectroscopy experiments were performed in a three-electrode electrochemical cell in which the PEDOT films coated GC electrodes were used as working electrodes. In these experiments, a CH Instruments a silver/silver chloride reference electrode with 1.0 M KCl filling solution was used as reference electrode and a GC rod served as counter electrode. The cyclic voltammetry experiments were performed in ferrocene methanol (FcMeOH) solutions of different concentrations with 0.1 M KCl as background electrolyte using scan rates between 25 and 200 mV/s. The impedance spectroscopy experiments were performed in the same three electrode cell filled with in 0.1 M KCl solution. The data were collected in the frequency range from 0.01Hz to 100 kHz at the

open circuit potential of the electrodes using a CH Instruments Electrochemical Workstation in combination with the CHI Version 18.01 software.

FTIR-ATR Spectroscopy (Figure 3d): To characterize the distribution of NCs in PEDOT films following different deposition protocols, an IFS 66/S FTIR spectrometer (Bruker Inc.) was used in junction with a Seagull variable angle reflection accessory and a Zinc Selenide hemispherical crystal (Harrick Scientific Products) for variable angle FTIR-ATR measurements. Variable angle measurements were collected by pressing the conductive polymer films deposited on ITO coated glass slides to the surface of the crystal with an applied torque of 920 g·cm. A schematic representation of how the samples were pressed against the ZnSe crystal is shown in Figure 3d. Generally, 64 interferograms were recorded with a deuterated triglycine sulfate detector and a resolution of 4 cm^{-1}. FTIR-ATR spectra of the NCs alone were collected by applying a small amount of dried NCs to a VideoMVP single reflection element diamond ATR accessory (Harrick Scientific Products) using the same parameters as in the variable angle measurements.

The penetration depth was calculated by Equation 1.[23]

$$d = \frac{\lambda}{2\pi n_1 \sqrt{\sin^2\theta - \left(\frac{n_2}{n_1}\right)^2}} \qquad \text{(Eq. 1)}$$

where d is the penetration depth, and λ, θ, n_1 and n_2 are the wavelength, incident angle, and the refractive indices of ATR crystal and sample, respectively. A refractive index of 2.414 was used for ZnSe crystal.[24] Since the refractive index of the PEDOT(TPFPhB)/NC films is a function of its composition,[25] the true refractive index of the PEDOT films was unknown. A value of 1.5 was used for this analysis as PEDOT(PSS) is often quoted as having a refractive index between 1.4 and 1.6.[26-27] The absorbance values at a characteristic wavenumber were determined as the

difference between the peak absorbance value and the absorbance value at the base of the peak.

X-ray Photoelectron Spectroscopy (XPS): XPS analysis of the distribution of the potentiostatically deposited NCs in PEDOT(TPFPhB) films was performed using a Thermo Scientific K-Alpha XPS system equipped with a monochromatic Al Kα X-ray source at 1486.6 eV. A spot size of 400 μm^2 was used with an X-ray power of 75 W at 12 kV. The instrument was calibrated to give binding energies of 84.0 eV for Au 4f7/2 and 284.6 eV for the C1s line of adventitious (aliphatic) carbon present on the non-sputtered samples. For depth profiling, an Ar^+ gun, with 3000 eV etching energy and 180 s etching times was used. Between the 19 etching steps, a series of XPS spectra were collected: high-resolution spectra of C 1s, S 2p, and Fe 3p were taken with 40 eV pass energy. The high-resolution scans were collected with an energy step size of 0.1 eV. The XPS data acquisition and analysis were performed using the Avantage software package.

Results and Discussion

In our previous paper,[19] we demonstrated the galvanostatic co-deposition EDOT-decorated NCs into a PEDOT film. The distribution of NCs in the PEDOT film was followed by XPS depth profiling using Ar^+ etching and iron(II) tris(bipyridine) complex inside the NCs as a marker. The iron(II) tris(bipyridine) complex, has been in-situ synthesized inside of the interior of the NCs with porous walls (see page 6330 in our previous paper[19]) prior to their co-polymerization with free EDOT. In this work, we expand the characterization of PEDOT films with immobilized NCs using variable angle FTIR-ATR spectroscopy.

In Figure 3, we show three different deposition methods for coupling the EDOT-decorated NCs to PEDOT films. The galvanostatic co-deposition of a PEDOT film with the EDOT-decorated NCs over a Au electrode surface in the presence of free EDOT molecules and tetrakis-(pentafluorophenyl)borate ($TPFPhB^-$) doping anions is termed as *bulk deposition* (Figure 3a). In contrast, when the EDOT-decorated NCs are deposited over an existing PEDOT film we speak about *surface deposition*. In this work we tested two surface deposition methods: (i) galvanostatic co-deposition EDOT-decorated NCs over an existing PEDOT film in the presence of free EDOT molecules and $TPFPhB^-$ doping anions (Figure 3b), which is termed bilayer deposition and (ii) potentiostatic immobilization of EDOT-decorated NCs to the surface of an existing PEDOT film in the presence of $TPFPhB^-$ doping anions but the absence of free EDOT molecules (Figure 3c). These deposition methods are expected to expand the potential applications of the hollow NCs for the development of modified electrodes with reagent loaded NCs in the bulk (Figure 3a) or on the surface of their sensing layers (Figure 3b and c).

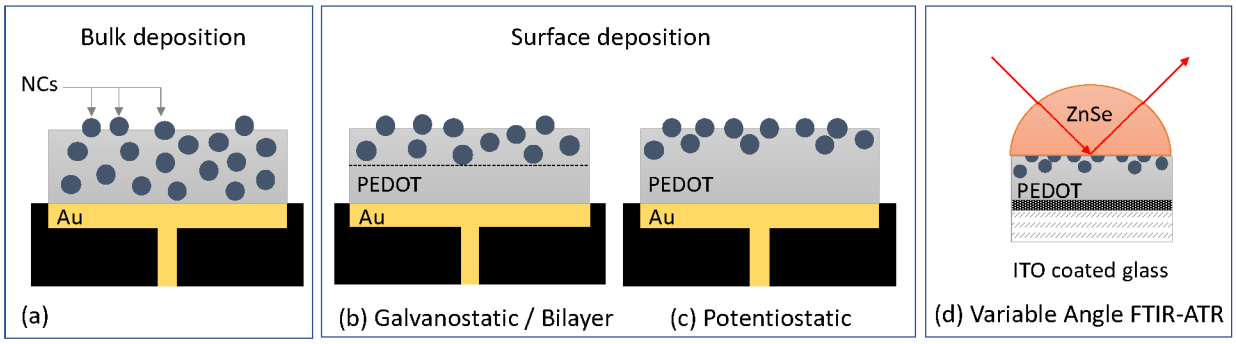

Figure 3: Schematic representation of bulk (a) and surface (b and c) deposition methods of EDOT-decorated NCs to a PEDOT(TPFPhB) film as supporting matrix and the schematic representation of how the distribution of NCs in the deposited films were determined with Variable Angle FTIR-ATR depth profiling experiments (d).

Electrochemical characterization of PEDOT(TPFPhB) films

In our experiments PEDOT(TPFPhB) is used as supporting conductive polymer matrix for the covalent attachment of the EDOT-decorated NCs due to the unique electrochemical properties of the PEDOT(TPFPhB) coated glassy carbon electrode (GC). The PEDOT(TPFPhB) coated GC electrode has about two orders of magnitude smaller capacitance ($C_{DL} < 5\ \mu F$) than the GC electrodes coated with PEDOT(PSS) (C_{DL}~$500\ \mu F$) or PEDOT(Cl) (C_{DL}~$400\ \mu F$). As we show in Figure 4a and 4b, the PEDOT(TPFPhB) coated GC electrode has almost identical behavior to the uncoated GC electrode in cyclic voltammetry (CV) experiments recorded in ferrocene methanol (FcMeOH) solutions. The peak currents increased linearly with the concentration (Figure 4e) and the peak separation, corresponding to the oxidation and reduction of FcMeOH was 57.0 mV (theoretical 57.8 mV) for both electrodes. The peak currents also increased linearly with the square root of the scan rate ($v^{1/2}$) (Figure 4f). The electrochemical surface areas, calculated from the slope of the i vs $v^{1/2}$ plot, were identical and agreed with the geometrical surface areas of the two electrodes.[19] In contrast, the cyclic voltammograms recorded with the PEDOT(PSS) (Figure 4c) and PEDOT(Cl) (Figure 4d) coated GC electrodes are dominated by the charging current of the capacitance of the PEDOT film[28-29] and the concentration dependence of the Faradaic-current is hardly recognizable. The differences in the electrochemical properties of PEDOT(PSS) and PEDOT(TPFPhB) coated electrodes are also conspicuous in the complex impedance plots of these electrodes. The results of the impedance analysis are summarized in Figure S4 of the supplementary information.

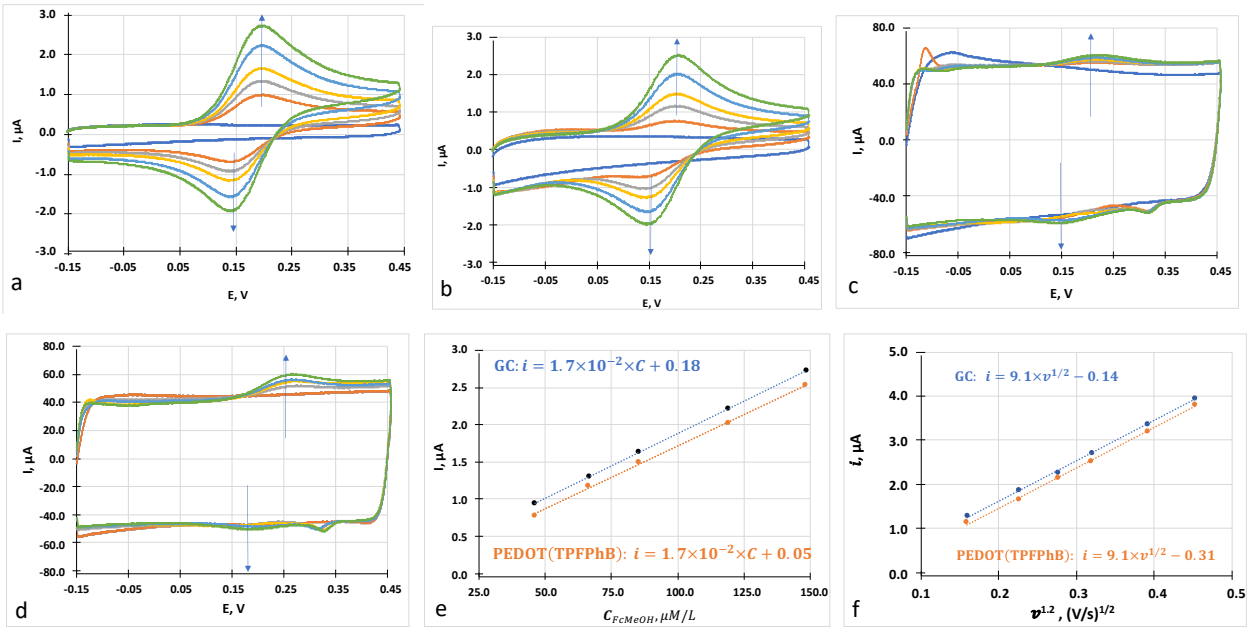

Figure 4: Cyclic voltammograms (CVs) recorded with a bare (a) GC electrode and GC electrodes coated with (b) PEDOT(TPFPhB), (c) PEDOT(PSS) and (d) PEDOT(Cl) in 0.1 M KCl background electrolyte and ferrocene methanol solutions with 45.9, 66.1, 84.7, 118, and 147 μM concentrations in the same background. The arrows in (a-d) show the effect of increasing concentrations. (e) Calibration curves constructed from the peak currents of the bare GC and the PEDOT(TPFPhB) coated electrodes. (f) Scan rate dependence of the peak currents (i vs. $v^{1/2}$) in 147 μM FcMeOH solution of the bare GC and the PEDOT(TPFPhB) coated electrodes. The calibration curves were recorded at with 100 mV/s scan rate. To construct the curves in (f) CVs were recorded at 25, 50, 75, 100, 150 and 200 mV/s scan rates. All the measurements were performed in combination with a 1.0 M KCl filled Ag/AgCl reference electrode and a GC rod as counter electrode.

Consequently, with the objective of utilizing the reagent loaded NCs for the potential development of novel electrochemical sensors, PEDOT(TPFPhB) was used as a supporting matrix for the immobilization of the EDOT-decorated NCs. Here we investigated the possibility of depositing the EDOT-decorated NCs predominantly to the surface of existing PEDOT(TPFPhB)

films. We attempted these depositions both in the presence and absence of EDOT molecules in the deposition solution. With EDOT in the polymerization solution the EDOT-decorated NCs are co-deposited with PEDOT(TPFPhB) over a GC electrode (Figure 3a) or over a previously deposited PEDOT(TPFPhB) film on the top of a GC electrode (Figure 3b). We termed these galvanostatic deposition protocols as “bulk” and “bi-layer” deposition, respectively. Without free EDOT in the polymerization solution, it was assumed, that the protruding EDOT moieties on the surface of the NCs could be oxidized and couple to the existing PEDOT(TPFPhB) film as a thin surface layer of NCs. The deposition of the EDOT-decorated NCs without EDOT in the solution was performed potentiostatically (Figure 3c).

FTIR-ATR and XPS Characteristics of EDOT-decorated Nanocapsules in PEDOT(TPFPhB) films.

For analyzing the distribution of NCs in the deposited films, variable angle FTIR-ATR spectroscopy and XPS depth profiling with Ar^+ etching was used. The FTIR-ATR spectra of PEDOT(TPFPhB) and acrylate-based NCs, shown in Figure 5, were used to identify the characteristic absorbance peaks that could be used to track the distribution of NCs in the conductive polymer films. In the PEDOT(TPFPhB) spectrum the absorbance bands at 1627, 1466, and 1273 cm^{-1} are assigned to C=C stretching, C-C stretching, and inter-ring stretching of the C-C bonds, respectively. The bands at 1158, 1122, 1074, 1018 and 997 cm^{-1} are attributed to the C-O-C vibration in the ethylenedioxy ring, and the bands at 948, 865, and 709 cm^{-1} are the characteristic stretching bands of the thiophene ring.[30-33] The prominent peaks in the FTIR-ATR spectrum of the acrylate-based NCs (Figure 5a, blue line) at 1720 and 1150 cm^{-1} are assigned to

the C=O and C-O stretching for the ester functional group, respectively, and the peak at 1460 cm^{-1} is assigned to the C-H bending. The ester absorbance peak at 1720 cm^{-1} appear to be adequate for tracing the NCs in the PEDOT film. On the other hand, the utility of the absorbance peaks at 1150 cm^{-1} and 1460 cm^{-1} in the spectrum of the acrylate-based NCs for quantification is questionable, due to the proximity of the absorbance bands in the PEDOT(TPFPhB) spectrum at 1158 cm^{-1} and 1466 cm^{-1}. To assess the expected change in the FTIR-ATR spectrum of PEDOT(TPFPhB) with increasing concentration of acrylate-based NCs on its surface, a series of simulated spectra were generated. In these simulations the absorbance values in the spectrum of the acrylate-based NCs (Figure 5a, blue line) were added in increasing proportion to the absorbance values in the PEDOT(TPFPhB) spectrum (Figure 5 brown line) according to the following expression:

$$A = A_{PEDOT} + xA_{nanocapsules} \quad \text{(Eq. 2)}$$

where A is the expected absorbance of PEDOT(TPFPhB) film at different levels of NC-loading, A_{PEDOT} and $A_{nanocapsules}$ are the principle absorbances of PEDOT and the NCs, respectively, and x is a coefficient used to simulate the influence of increasing NC concentration in the PEDOT film on the FTIR-ATR spectra. The three important regions of the resulting spectra are shown in Figure 5b-d.

Based on Figure 5b and 5c the acrylate specific peaks at 1720 and 1460 cm^{-1}, appear to be adequate to identify the presence of NCs in a PEDOT/NC copolymer film with more or less sensitivity ($\Delta A_{max}^{1720} = 96.1\ mAU$ and $\Delta A_{max}^{1460} = 16.3\ mAU$), respectively. In our analysis, the overlap from the PEDOT spectra was more significant at the 1150 cm^{-1} band. Since the measured spectra of the copolymer films are complex, to compensate for variability in the films

an internal reference peak was chosen at 976 cm^{-1}, with an absorbance which is relativity independent from changing NC concentration in the copolymer film ($\Delta A_{max}^{976} = 0.56\, mAU$, Figure 5d).

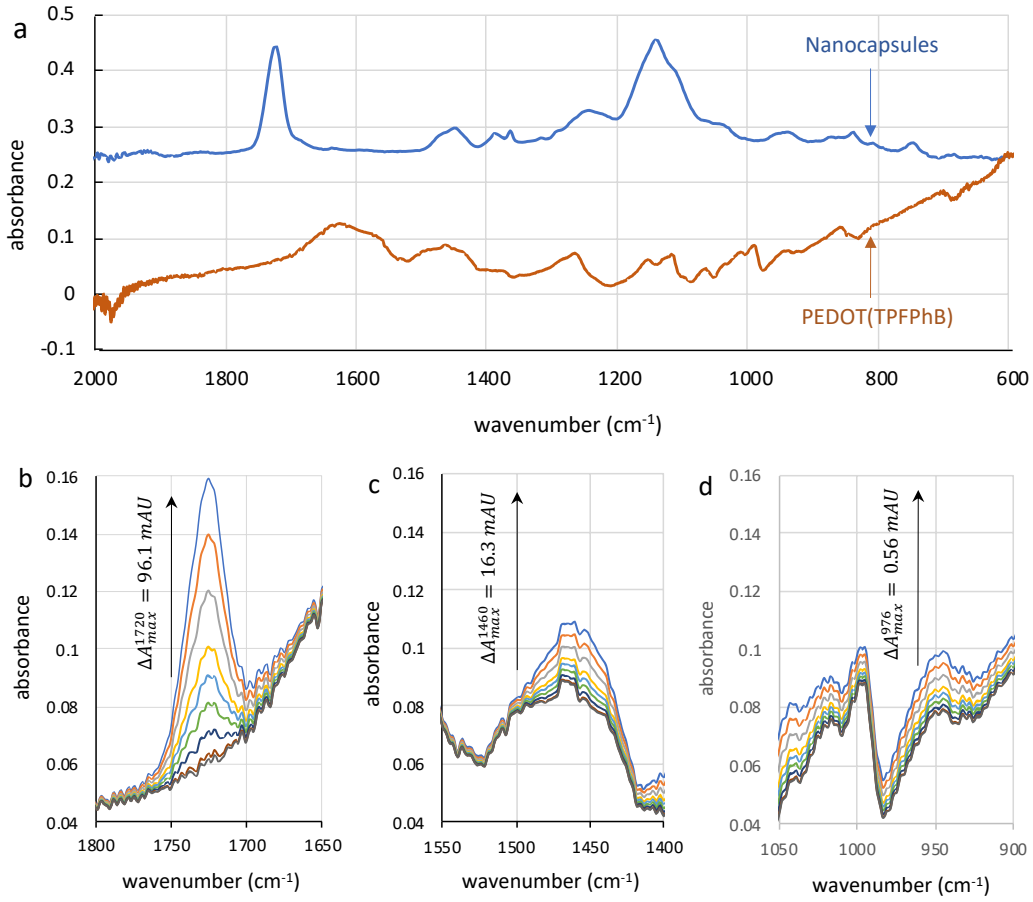

Figure 5. (a) FTIR-ATR spectra of PEDOT(TPFPhB) and polyacrylate-based NCs on ITO coated glass slide. PEDOT(TPFPhB) was galvanostatically deposited while the polyacrylate-based NCs were drop cast and dried to the ITO surface. The spectra were shifted along the absorbance axis for better comparison. (b-d) Spectral regions of interest in simulated FTIR-ATR spectra constructed with Eq. 2 with x = 0, 0.01, 0.05, 0.1, 0.15, 0.2, 0.3, 0.4, and 0.5. ΔA_{max} is the difference in absorbance at the indicated wavenumbers of the absorbance peaks for x = 0.5 and x=0 in Eq. 2.

Comparison of Bulk and Surface Deposition Methods.

In this paper, we speak about galvanostatic bulk and bilayer deposition protocols when the EDOT-decorated NCs are deposited in the presence of free EDOT molecules. As shown schematically in Figure 3, upon the implementation of these protocols the EDOT-decorated NCs are incorporated in a gradually growing PEDOT(TPFPhB) film on a gold electrode surface (bulk deposition, Figure 3a) or on the top of an existing PEDOT(TPFPhB) film (bilayer deposition, Figure 3b). Depth profiling with variable angle FTIR-ATR spectroscopy allows for the comparison of the distribution of NCs in PEDOT(TPFPhB) films deposited with the bulk and bilayer deposition protocols. The FTIR-ATR spectra of these films were measured at angles ranging from 39^{o} to 60^{o} using a hemispherical ZnSe crystal corresponding to penetration depths between 3.84 to 0.64 μm at 1720 cm^{-1}. The collected spectra for the bulk and bilayer deposited films are shown in Figure 6.

The gradual increase of the absorbance values with decreasing angle, best seen at lower wavenumbers, is the consequence of the increasing penetration depth. The incorporation of the EDOT-decorated NCs into the electrochemically deposited films is confirmed by the characteristic ester peak of the NCs at 1720 cm^{-1} in both spectra. Figure 7 shows the results of our analysis on the distribution of NCs in the PEDOT(TPFPhB) films, deposited by the bulk and bilayer deposition protocols using the characteristic peaks at 1720 cm^{-1} and 1460 cm^{-1}. Due to the more significant overlap from the PEDOT spectra the results of the same analysis using the 1150 cm^{-1} band was more difficult to interpret.

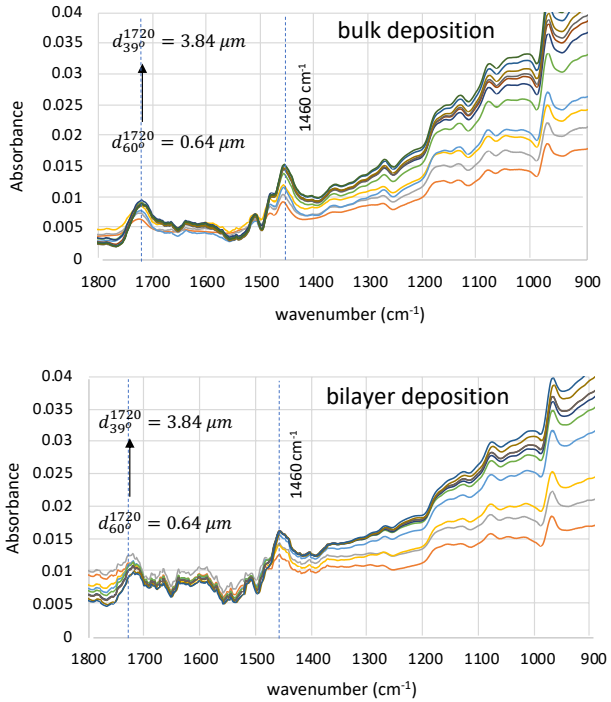

Figure 6. FTIR-ATR spectra of EDOT-decorated NCs deposited by the bulk (top) and bilayer (bottom) deposition methods into PEDOT(TPFPhB) films. The FTIR-ATR spectra of these films were measured at angles ranging from 39° to 60° using a hemispherical ZnSe crystal corresponding to penetration depths between 3.84 to 0.64 μm at 1720 cm^{-1}.

Figure 7a and c show the change in absorbance with increasing penetration depth at 1460 cm^{-1} and 1720 cm^{-1} for both the bulk and bilayer deposited films. According to Beer-Lambert law, the absorbance is expected to increase linearly with the penetration depth in a homogeneous film with a slope of molar absorptivity times concentration. In the bulk deposited film, in which the NCs are assumed to be distributed homogenously, the absorbance indeed increases linearly at low penetration depth values. Since the film thickness is about 1 μm, as the penetration depth approaches the film thickness, the absorbance value approaches a saturation value corresponding to the 1 μm film thickness and NC concentration in the film. Deviations from a linear increase in the absorbance above ~ 0.7 μm penetration depth is likely

due to deviations in the NC distribution at the polymer-electrode interface compared to the bulk of the deposited film.

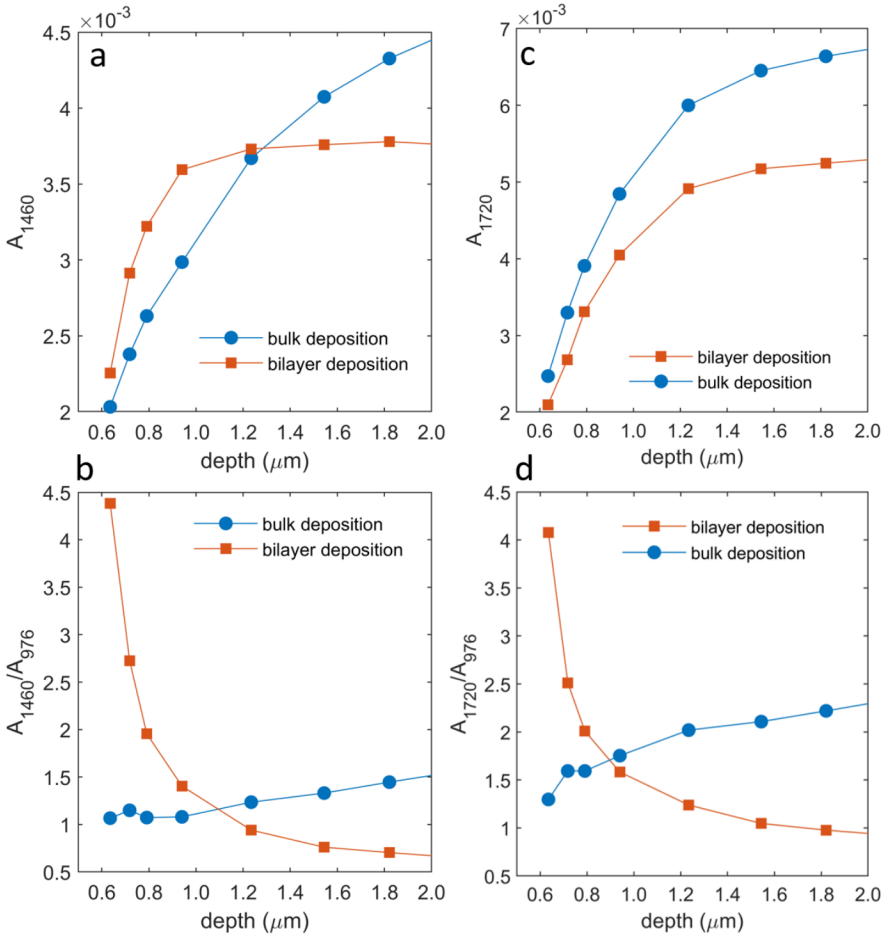

Figure 7 (a and c): Change in absorbance with increasing penetration depth in FTIR-ATR spectroscopy at 1460 cm^{-1} (a) and 1720 cm^{-1} (c) wavenumbers in PEDOT(TPFPhB) films deposited with the bulk and bilayer deposition protocols. The curves were constructed from the spectra shown in Figure 6. (b and d): Change in absorbance ratios A_{1460}/A_{976} (b) and A_{1720}/A_{976} (d) in FTIR-ATR spectroscopy with increasing penetration depth for the bulk and bilayer deposited films. The absorbance ratios were calculated for the peaks at 1460 and 1720 cm^{-1} with respect to the internal reference peak at 976 cm^{-1} which was shown to be independent of the NC concentration.

In contrast to the film deposited with the bulk deposition protocol, NCs are expected to be present only in the ~0.5 μm thick top layer of the film deposited with the bilayer protocol. This ~0.5 μm thick NC-loaded layer was deposited over the underlying NC-free PEDOT(TPFPhB) film. Consequently, the absorbance values recorded at variable angles are expected to increase linearly only up to ~0.5 μm penetration depth, where the penetrating IR beam reaches the boundary between the NC-loaded and NC-free PEDOT(TPFPhB) films. Beyond, 0.5 μm penetration depth the absorbance is expected to remain constant. Figure 7a is in agreement with these expectations. As seen in Figure 7a, the absorbance increases until a penetration depth of ~0.8 μm, which is slightly deeper than the thickness of the NC-loaded copolymer layer which was deposited on the top of an existing 1 μm NC-free PEDOT(TPFPhB) film. After ~0.8 μm the absorbance remained constant with increasing penetration depths. In Figure 7c we show the results of the same analysis on the 1720 cm^{-1} peak. The conclusion of this analysis is the same although the difference in the shapes of the curves representing the bulk and bilayer deposition protocols are less obvious than in Fig 7a. However, the penetration depths, where the absorbance values start to deviate from the linear increase and reach saturation, are both smaller for the film deposited with the bilayer protocol. Moreover, in agreement with the expectations, the maximum value of the film absorbance is significantly smaller in the samples deposited with the bilayer (~0.5 μm) than with the bulk (~1.0 μm) protocol. The difference between the depth where the interface between the NC free and NC loaded layers is expected (0.5 μm) and observed, is the consequence of the highly porous structure and large pore sizes in the PEDOT(TPFPhB) film compared to the diameters of the NCs (~170 nm) incorporated into the film. Based on the images shown in Figure 2 and Figure S1 in the Supporting Information, it

is feasible that during the deposition procedure a significant number of NCs diffuse into the pores and are embedded in the deeper layers of the existing PEDOT(TPFPhB) film resulting in a less well-defined interface.

Using the peak at 976 cm^{-1}, which was shown to be independent of the NC concentration, as an internal reference, in Figure 7b and d, we show the change in the A_{1460}/A_{976} and A_{1720}/A_{976} absorbance ratios as a function of the penetration depth. As can be seen in Figures 7b and d, at low penetration depth values, these absorbance ratios are significantly larger for the film deposited with the bilayer deposition protocol compared to the film deposited with the bulk deposition protocol. Moreover, the A_{1460}/A_{976} and A_{1720}/A_{976} absorbance ratios for the films deposited with the bilayer protocol decay very quickly with the increasing penetration depth and remain essentially constant once the penetration depth exceeded 0.5 µm, the interface between the PEDOT(TPFPhB) and the NC-containing PEDOT(TPFPhB) films. In contrast, the same ratios in the bulk deposited films are almost constant or are slightly increasing. The significant difference in the traces confirms that the bilayer deposition method results in a film with significantly larger NCs concentration in its top layer compared to underlaying PEDOT(TPFPhB) film, which has been deposited in the absence of EDOT-decorated NCs.

Comparison of Galvanostatic and Potentiostatic Deposition Methods

Beyond the galvanostatic bilayer deposition method for constructing a NC-rich layer on the surface of an existing PEDOT(TPFPhB) film, an alternative deposition protocol was also evaluated. We attempted to deposit the EDOT-decorated NCs over a 1 µm thick galvanostatically deposited PEDOT(TPFPhB) layer using a potentiostatic deposition protocol

without free EDOT in the deposition solution. The current vs. time curve recorded during the deposition is shown in Figure S3 in the Supporting Information (Applied potential: 0.925V vs. Ag/AgCl/1.0 M KCl; Electrolysis time: 1200 s). To evaluate the efficiency of the potentiostatic deposition protocol, FTIR-ATR spectra were collected from the target surface with 35°, 45°, and 60° incident angles using a ZnSe hemispherical crystal (Figure 8a). As shown in Figure 8, with increasing penetration depth (decreasing angle of incidence) the absorbance increases at all wavenumbers. Although we did not have any specific information about the thickness of the potentiostatically deposited NC layer, it was assumed that the concentration of NCs on the surface of the electrode is significantly larger compared to the deeper layers of the PEDOT(TPFPhB) film. If the NC layer is deposited only to the utmost surface layer of the PEDOT(TPFPhB) film and is very thin, then the characteristic acrylate peak should not or only hardly increase with increasing penetration depth. To assess the concentration of NCs on the PEDOT(TPFPhB) film, similar to Figure 7b and d, the A_{1720}/A_{976} absorbance ratios were calculated at 1.13 and 0.64 µm penetration depth (corresponding to incident angles of 45° and 60°, respectively) and compared to the A_{1720}/A_{976} absorbance ratios in a film deposited with the bulk deposition protocol. The results are summarized in Table 1.

Table 1: A_{1720}/A_{976} ratios determined from the FTIR-ATR spectra of NC containing PEDOT(TPFPhB) films at different penetration depths. The films were deposited with the potentiostatic surface and galvanostatic bulk deposition protocols.

Penetration depth	A_{1720}/A_{976}	
	Surface deposited film	Bulk deposited film
1.13 µm	0.75	2
0.64 µm	0.43	1.6

The data in Table 1, suggests a lower average concentration of NCs in the film deposited with the surface deposition protocol compared to the bulk deposited film, which at first sight could be interpreted that the surface deposition protocol deposited only a very thin layer of NCs. However, the A_{1720}/A_{976} ratio increased similarly with the penetration depth in the surface and bulk deposited films. This suggests that the NCs deposited potentiostatically are not confined to the surface of the PEDOT(TPFPhB) film, but they also appear in the deeper layers of the PEDOT(TPFPhB) film which has been deposited in the absence of NCs. This finding has been confirmed by subtracting the FTIR-ATR spectrum collected at 60° (0.64 µm penetration depth) from the spectrum collected at 45° (1.13 µm penetration depth). The difference between two FTIR-ATR spectra $(A_{45^o} - A_{60^o})$ reflects the NC concentration in a ~ 0.49 µm thick PEDOT(TPFPhB) film, just below the top 0.64 µm thick surface layer.

As shown in Figure 8b, the absorbance in the difference spectra at the peak at 1720 cm^{-1} is approximately half of the value what was recorded at 45° (1.13 µm penetration depth), i.e., the NC concentration in the top 0.64 µm thick layer of the PEDOT(TPFPhB) film is very similar to the concentration in the 0.49 µm thick layer directly beneath it. This means, the potentiostatic deposition method does not lead to a NC-rich surface layer as it was hypothesized at the beginning of this work (Figure 3c). On the other hand, this finding supports our explanation of the diffusive interface between PEDOT films deposited by the bilayer deposition protocol with and without NCs.

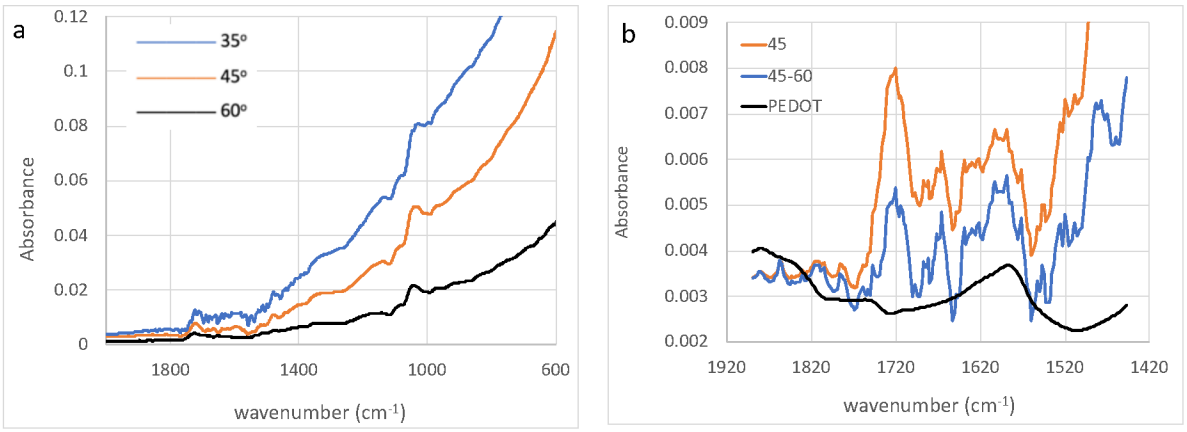

Figure 8. (a) Variable angle FTIR-ATR spectra of a ~ 1 µm thick PEDOT(TPFPhB) film to which EDOT-decorated NCs were deposited with the potentiostatic surface deposition protocol. The spectra were recorded with 35° (blue), 45° (orange) and 60° (black) incident angles using a ZnSe crystal. (b) blow-up fraction of FTIR-ATR spectra recorded at (i) 45° angle of incidence of a PEDOT(TPFPhB) film with EDOT-decorated NCs on its surface (orange line); (ii) the difference between two FTIR-ATR spectra $(A_{45^o} - A_{60^o})$, recorded on the same surface at 45° and 60° angle of incidence, i.e. between 1.13 µm and 0.64 penetration depth, respectively (blue line); and (iii) the FTIR-ATR spectrum of a PEDOT(TPFPhB) film without incorporated NCs (black line).

To confirm the results of the FTIR-ATR analysis, the distribution of the potentiostatically deposited NCs in PEDOT(TPFPhB) films was also measured by XPS. The XPS analysis required NCs which were loaded with compounds with characteristic binding energies. In this work for the XPS experiments, iron(II) bipyridine complex loaded NCs were used. The $Fe(bpy)_3$ complex was synthesized in situ in the interior of the porous NCs prior to the electrochemical deposition of the NCs into the PEDOT(TPFPhB) films. To determine the distribution of NCs in the surface layers of the PEDOT(TPFPhB) films XPS depth profiling with Ar^+ etching was used (19 etching intervals with 180 s etching times and 3000 eV energy). 180 s etching shaved off an approximately 60 nm thick layer from the top of the conductive polymer film. The results of the

depth profiling experiment are shown in Figure 9. After 19 etching cycles, the PEDOT(TPFPhB) film is completely etched from the underlaying Au electrode. According to Figure 9, the carbon, sulfur, and iron fitted areas all follow the same decaying pattern. These results suggest that the iron(II) bipyridine complex loaded NCs are present in the full cross-section of the PEDOT film which is in complete agreement with the conclusions of the FTIR-ATR analysis of the PEDOT(TPFPhB) films with potentiostatically deposited NCs on its surface.

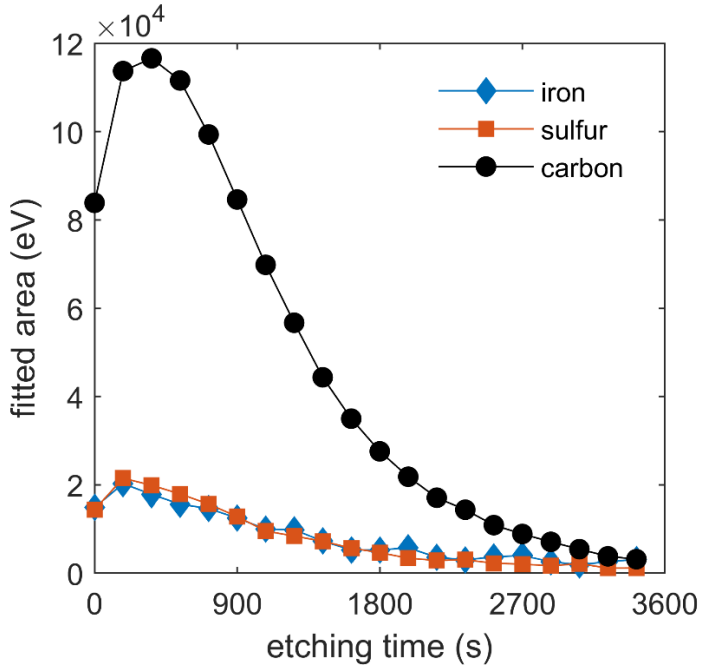

Figure 9. XPS depth-profiles of iron, sulfur, and carbon in PEDOT(TPFPhB) films with potentiostatically deposited, iron(II)tris(2-2'-bipyridine)-loaded NCs on an existing 1 µm thick PEDOT(TPFPhB) film. The individual data points were determined after 180 s, 3000 eV Ar^+ plasma etching cycles.

Considering the highly porous structure of PEDOT films, with pore sizes significantly larger than the average diameter (170 nm) of NCs synthesized in this study (see Figure S1 in the Supporting Information),[33] it is not surprising that NCs were identified in the deeper layers of the PEDOT(TPFPhB) film. The large applied potential (0.925 V vs. Ag/AgCl/sat. KCl) may have

contributed to the highly porous structure of the PEDOT film.[34] It was used to overcome the film resistance and allow the oxidation of the EDOT motifs located on the surface of the nanocapsules.

Conclusions

In this work, we investigated the deposition of EDOT-decorated NCs into the bulk, and onto the surface layer of PEDOT(TPFPhB) films. PEDOT(TPFPhB) was used as supporting conductive polymer matrix for the covalent attachment of the EDOT-decorated NCs due to the uniquely advantageous properties of PEDOT(TPFPhB) coated working electrodes in voltametric experiments. During the bulk deposition, the EDOT-decorated NCs were co-polymerized with free EDOT in the deposition solution onto the surface of a gold electrode or ITO coated glass slides using a galvanostatic deposition protocol. As surface deposition protocols both galvanostatic and potentiostatic deposition protocols were tested in the presence or absence of free EDOT in the polymerization solution, respectively. During surface deposition, the EDOT-decorated NCs were deposited over a ~ 1 μm thick, NC-free PEDOT(TPFPhB) films. The deposited films were studied using variable angle FTIR-ATR spectroscopy and XPS depth profiling to track the location of the NCs in the deposited films. With the galvanostatic surface deposition method bilayer structures were made, in which the interface between the NC-free and NC-loaded layers could be identified using FTIR-ATR, however, the interface was quite diffuse, likely due to the highly porous nature of the galvanostatically deposited PEDOT(TPFPhB) film. The FTIR-ATR and XPS analysis of the films deposited potentiostatically, in the absence of EDOT in the deposition solution, showed small amounts of NCs in the entire

cross-section of the films which supports the conclusion that the porous nature of PEDOT limits the possibility of the deposition of a compact NC-layer with a well-defined interface with an underlaying PEDOT(TPFPhB) film. The two fundamental questions related to the fate of the NCs during their galvanostatic/potentiostatic deposition are: (i) Do the NCs keep their integrity during their covalent attachment to a growing PEDOT film? (ii) Do the NCs become filled with PEDOT inside upon their copolymerization with free EDOT? With respect to the first question, both the SEM images and the XPS analysis of NC-loaded PEDOT films support the conclusion that the NCs remain intact during their electrochemical deposition. Regarding the second question, experimentally we could not demonstrate directly whether there is some PEDOT inside of the NCs because the chemical properties of PEDOT inside and outside of the NCs are assumed to be the same, and because the NCs are incorporated in a PEDOT film with the same chemical/spectroscopical properties.

In summary, the galvanostatic deposition of EDOT-decorated NCs was shown to produce structures loaded with NCs covalently attached to the PEDOT(TPFPhB) film. However, for practical sensor applications, the concentration of the NCs in the bulk or on the sensing surface must be increased through an improved NC deposition protocol, e.g., increasing EDOT moieties on the NC surfaces and increasing concentration of EDOT-decorated NCs in the deposition solution.

Acknowledgement

The Johan Gadolin scholarship that provided the financial support for Bradly Hambly to perform critical parts of the work at Åbo Akademi University is gratefully acknowledged.

Supporting information

The Supporting Information is available free of charge at

– SEM image of a ~ 1 µm thick copolymer of PEDOT(TPFPhB) and EDOT-decorated nanocapsules

– Potential vs. time curve recorded during the galvanostatic co-deposition of EDOT decorated nanocapsules with a PEDOT(TPFPhB) conductive polymer film

– Current vs. time curve collected during the potentiostatic deposition of the EDOT-decorated nanocapsules to 1 µm thick PEDOT(TPFPhB) film

– Electrochemical impedance spectroscopy plots of a bare GC and one PEDOT(PSS) and two PEDOT(TPFPhB) coated GC electrodes

References

1. Kim, M. D.; Dergunov, S. A.; Richter, A. G.; Durbin, J.; Shmakov, S. N.; Jia, Y.; Kenbeilova, S.; Orazbekuly, Y.; Kengpeiil, A.; Lindner, E.; Pingali, S. V.; Urban, V. S.; Weigand, S.; Pinkhassik, E., Facile Directed Assembly of Hollow Polymer Nanocapsules within Spontaneously Formed Catanionic Surfactant Vesicles. *Langmuir* **2014,** *30* (24), 7061-7069.
2. Danila, D. C.; Banner, L. T.; Karimova, E. J.; Tsurkan, L.; Wang, X.; Pinkhassik, E., Directed Assembly of Sub-Nanometer Thin Organic Materials with Programmed-Size Nanopores. *Angew. Chem. Int. Edit.* **2008,** *47* (37), 7036-7039.

3. Richter, A. G.; Dergunov, S. A.; Kim, M. D.; Shmakov, S. N.; Pingali, S. V.; Urban, V. S.; Liu, Y.; Pinkhassik, E., Unraveling the Single-Nanometer Thickness of Shells of Vesicle-Templated Polymer Nanocapsules. *J. Phys. Chem. Lett.* **2017,** *8* (15), 3630-3636.
4. Dergunov, S. A.; Pinkhassik, E., Synergistic Co-Entrapment and Triggered Release in Hollow Nanocapsules with Uniform Nanopores. *J. Am. Chem. Soc.* **2011,** *133* (49), 19656-19659.
5. Shmakov, S. N.; Jia, Y.; Pinkhassik, E., Selectively Initiated Ship-In-A-Bottle Assembly of Yolk–Shell Nanostructures. *Chem. Mater.* **2014,** *26* (2), 1126-1132.
6. Gustafson, T. P.; Dergunov, S. A.; Akers, W. J.; Cao, Q.; Magalotti, S.; Achilefu, S.; Pinkhassik, E.; Berezin, M. Y., Blood Triggered Rapid Release Porous Nanocapsules. *RSC Adv.* **2013,** *3* (16), 5547-5555.
7. Zhegalova, N. G.; Dergunov, S. A.; Wang, S. T.; Pinkhassik, E.; Berezin, M. Y., Design of Fluorescent Nanocapsules as Ratiometric Nanothermometers. *Chem-Eur J* **2014,** *20* (33), 10292-10297.
8. Maclin, A. Q.; Kim, M. D.; Dergunov, S. A.; Pinkhassik, E.; Lindner, E., Small-Volume pH Sensing with a Capillary Optode Utilizing Dye-Loaded Porous Nanocapsules in a Hydrogel Matrix. *Electroanal.* **2015,** *27* (3), 733-744.
9. Dergunov, S. A.; Khabiyev, A. T.; Shmakov, S. N.; Kim, M. D.; Ehterami, N.; Weiss, M. C.; Birman, V. B.; Pinkhassik, E., Encapsulation of Homogeneous Catalysts in Porous Polymer Nanocapsules Produces Fast-Acting Selective Nanoreactors. *ACS Nano* **2016,** *10* (12), 11397-11406.
10. Dergunov, S. A.; Miksa, B.; Ganus, B.; Lindner, E.; Pinkhassik, E., Nanocapsules with "Invisible" Walls. *Chem. Comm.* **2010,** *46* (9), 1485-1487.
11. Socaci, C.; Rybka, M.; Magerusan, L.; Nan, A.; Turcu, R.; Liebscher, J., Magnetite Nanoparticles Coated With Alkyne-Containing Polyacrylates for Click Chemistry. *J. Nanopart. Res.* **2013,** *15* (6), 1747.
12. Campos, M. A. C.; Paulusse, J. M.; Zuilhof, H., Functional Monolayers on Oxide-Free Silicon Surfaces via Thiol–Ene Click Chemistry. *Chem. Comm.* **2010,** *46* (30), 5512-5514.

13. Urbanowicz, M.; Pijanowska, D. G.; Jasiński, A.; Ekman, M.; Bocheńska, M. K., A Miniaturized Solid-Contact Potentiometric Multisensor Platform for Determination of Ionic Profiles in Human Saliva. *J. Solid State Electr.* **2019,** *23* (12), 3299-3308.
14. Wang, G.; Morrin, A.; Li, M.; Liu, N.; Luo, X., Nanomaterial-Doped Conducting Polymers for Electrochemical Sensors and Biosensors. *J. Mater. Chem. B* **2018,** *6* (25), 4173-4190.
15. Bobacka, J., Potential Stability of All-Solid-State Ion-Selective Electrodes Using Conducting Polymers as Ion-to-Electron Transducers. *Anal. Chem.* **1999,** *71* (21), 4932-4937.
16. Bobacka, J.; Ivaska, A.; Lewenstam, A., Potentiometric Ion Sensors Based on Conducting Polymers. *Electroanal.* **2003,** *15* (5-6), 366-374.
17. Lindner, E.; Gyurcsányi, R. E., Quality Control Criteria for Solid-Contact, Solvent Polymeric Membrane Ion-Selective Electrodes. *J. Solid State Electr.* **2009,** *13* (1), 51-68.
18. Bobacka, J.; Ivaska, A.; Lewenstam, A., Potentiometric Ion Sensors. *Chem. Rev.* **2008,** *108* (2), 329-351.
19. Hambly, B.; Guzinski, M.; Perez, F.; Pendley, B.; Lindner, E., Synthesis and Deposition of EDOT-Decorated Hollow Nanocapsules into PEDOT Films for Optical and Electrochemical Sensing. *ACS Appl. Nanomat.* **2020,** *3* (7), 6328-6335.
20. Qin, L.; Xu, J.; Lu, B.; Lu, Y.; Duan, X.; Nie, G., Synthesis and Electrochromic Properties of Polyacrylate Functionalized Poly(3,4-Ethylenedioxythiophene) Network Films. *J. Mat. Chem.* **2012,** *22* (35), 18345-18353.
21. Mouffouk, F.; Higgins, S. J., Oligonucleotide–Functionalised Poly(3,4-Ethylenedioxythiophene)-Coated Microelectrodes which Show Selective Electrochemical Response to Hybridisation. *Electrochem. Comm.* **2006,** *8* (2), 317-322.
22. Guzinski, M.; Jarvis, J. M.; Perez, F.; Pendley, B. D.; Lindner, E.; De Marco, R.; Crespo, G. A.; Acres, R. G.; Walker, R.; Bishop, J., PEDOT(PSS) as Solid Contact for Ion-Selective Electrodes: The Influence of the PEDOT(PSS) Film Thickness on the Equilibration Times. *Anal. Chem.* **2017,** *89* (6), 3508-3516.
23. Urbaniak-Domagala, W., The Use of the Spectrometric Technique FTIR-ATR to Examine the Polymers Surface. *Adv Asp. Spectr.* **2012,** *3*, 85-104.

24. Querry, M., *Optical Constants of Minerals and Other Materials from the Millimeter to the Ultraviolet*. Defense Tech. Inform. Center University of MIissouri - Kansas City, 1987; p 83.
25. Bergman, D. J., The Dielectric Constant of a Composite Material—A Problem in Classical Physics. *Phys. Rep.* **1978,** *43* (9), 377-407.
26. Elschner, A.; Kirchmeyer, S.; Lovenich, W.; Merker, U.; Reuter, K., *PEDOT: Principles and Applications of an Intrinsically Conductive Polymer*. CRC Press: Boca Raton, 2010; p 142.
27. Yang, Z.; Fang, Z.; Sheng, J.; Ling, Z.; Liu, Z.; Zhu, J.; Gao, P.; Ye, J., Optoelectronic Evaluation and Loss Analysis of PEDOT:PSS/Si Hybrid Heterojunction Solar Cells. *Nanoscale Res Lett* **2017,** *12* (1), 26.
28. Bobacka, J.; Lewenstam, A.; Ivaska, A., Electrochemical Impedance Spectroscopy of Oxidized Poly(3,4-Ethylenedioxythiophene) Film Electrodes in Aqueous Solutions. *J. Electroanal. Chem.* **2000,** *489* (1), 17-27.
29. Dkhissi, A.; Louwet, F.; Groenendaal, L.; Beljonne, D.; Lazzaroni, R.; Brédas, J. L., Theoretical Investigation of the Nature of the Ground State in the Low-Bandgap Conjugated Polymer, Poly(3,4-Ethylenedioxythiophene). *Chem. Phy. Lett.* **2002,** *359* (5-6), 466-472.
30. Kvarnström, C.; Neugebauer, H.; Ivaska, A.; Sariciftci, N. S., Vibrational Signatures of Electrochemical p- and n-Doping of Poly(3,4-Ethylenedioxythiophene) Films: An in Situ Attenuated Total Reflection Fourier Transform Infrared (ATR-FTIR) Study. *J. Mol. Struct.* **2000,** *521* (1-3), 271-277.
31. Kvarnström, C.; Neugebauer, H.; Blomquist, S.; Ahonen, H. J.; Kankare, J.; Ivaska, A., In Situ Spectroelectrochemical Characterization of Poly(3,4-Ethylenedioxythiophene). *Electrochim. Acta* **1999,** *44* (16), 2739-2750.
32. Zhao, Q.; Jamal, R.; Zhang, L.; Wang, M.; Abdiryim, T., The Structure and Properties of PEDOT Synthesized by Template-Free Solution Method. *Nanoscale Res Lett* **2014,** *9* (1), 557.
33. Patra, S.; Barai, K.; Munichandraiah, N., Scanning Electron Microscopy Studies of PEDOT Prepared by Various Electrochemical Routes. *Synthetic Met.* **2008,** *158* (10), 430-435.
34. Hui, Y.; Bian, C.; Wang, J.; Tong, J.; Xia, S., Comparison of Two Types of Overoxidized PEDOT Films and Their Application in Sensor Fabrication. *Sensors (Basel)* **2017,** *17* (3), 628.

TOC figure

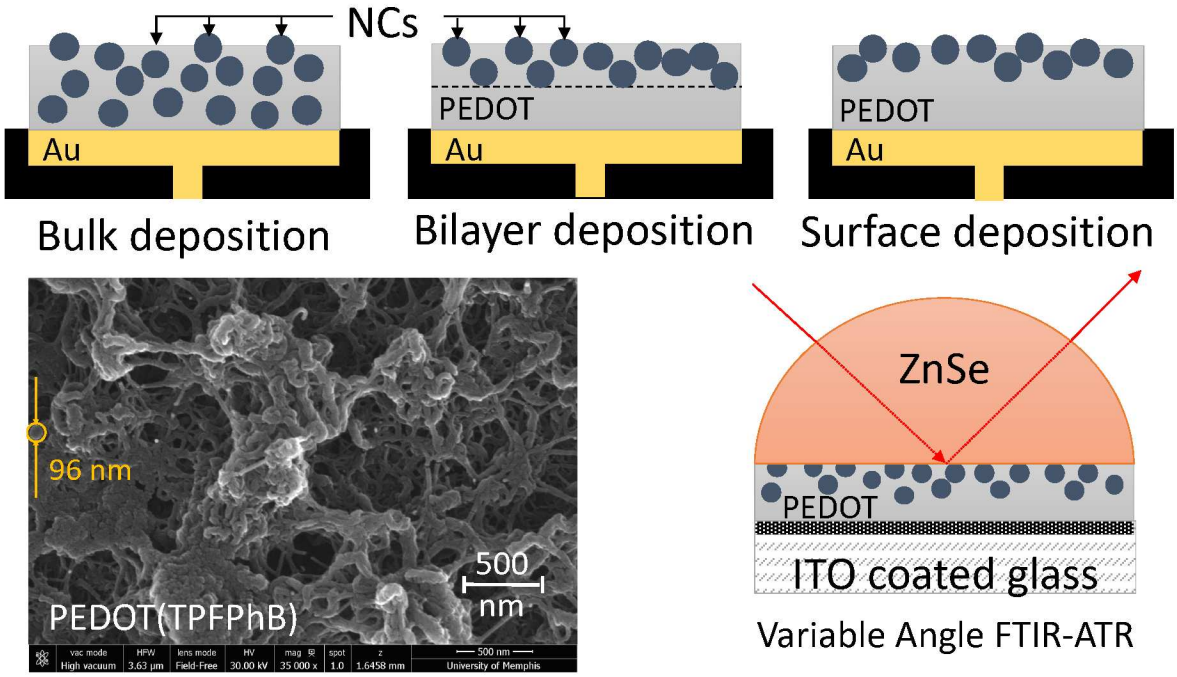

TOC 3.25” × 1.75”

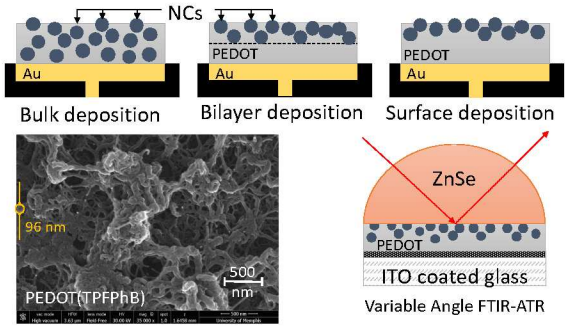

Au
NCs
Bulk deposition
PEDOT
Au
Bilayer deposition
PEDOT
Au
Surface deposition
ZnSe
PEDOT
ITO coated glass
Variable Angle FTIR-ATR
96 nm
500 nm
PEDOT(TPFPhB)
vac mode High vacuum
HFW 3.63 µm
lens mode Field Free
HV 30.00 kV
mag 35 000 x
spot 1.0
z 1.6458 mm
500 nm
University of Memphis